Behavioral/Systems/Cognitive

Temporal Dynamics and Latency Patterns of Receptor Neuron Input to the Olfactory Bulb

Hartwig Spors,[1]* Matt Wachowiak,[3,4]* Lawrence B. Cohen,[3] and Rainer W. Friedrich[2]

[1]WIN Group of Olfactory Dynamics and [2]Department of Biomedical Optics, Max-Planck-Institut für Medizinische Forschung, D-69120 Heidelberg, Germany, [3]Department of Cellular and Molecular Physiology, Yale University School of Medicine, New Haven, Connecticut 06520, and [4]Department of Biology, Boston University, Boston, Massachusetts 02215

Odorants are first represented in the brain by distributed patterns of activity in the olfactory bulb (OB). Although neurons downstream of sensory inputs respond to odorants with temporally structured activity, sensory inputs to glomeruli are typically described as static maps. Here, we imaged the temporal dynamics of receptor neuron input to the OB with a calcium-sensitive dye in the olfactory receptor nerve terminals in anesthetized mice. We found that diverse, glomerulus- and odorant-dependent temporal dynamics are present even at this initial input stage. Instantaneous spatial patterns of receptor input to glomeruli changed both within and between respiration cycles. Glomerular odorant responses differed in amplitude, latency, rise time, and degree of modulation by sniffing in an odorant-specific manner. Pattern dynamics within the first respiration cycle recurred in a similar manner during consecutive cycles. When sniff rate was increased artificially, pattern dynamics were preserved in the first sniff but were attenuated during subsequent sniffs. Temporal response properties were consistent across individuals on a coarse regional scale and on a fine scale of individual glomeruli. Latency and magnitude of glomerular inputs were only weakly correlated and might therefore convey independent odorant information. These data demonstrate that glomerular maps of primary sensory input to the OB are temporally dynamic. These dynamics may contribute to the representation of odorant information and affect information processing in the central olfactory system of rodents.

Key words: **olfaction; sensory coding; imaging; *in vivo*; mouse; maps**

Introduction

Olfactory stimuli (odorants) are initially represented in the brain by patterns of activity across the glomeruli of the olfactory bulb (OB) (Leveteau and MacLeod, 1966; Stewart et al., 1979; Guthrie et al., 1993; Friedrich and Korsching, 1997; Luo and Katz, 2001; Wachowiak and Cohen, 2001; Laurent, 2002; Spors and Grinvald, 2002). In mice, each of ~2000 glomeruli receives sensory input from ~4000 olfactory receptor neurons (ORNs) expressing the same odorant receptor (Ressler et al., 1994; Vassar et al., 1994; Mombaerts et al., 1996). Inputs converging to one glomerulus respond to odorants with similar specificity and time course (Bozza et al., 2002; Wachowiak et al., 2004), suggesting that they constitute functional units (Hildebrand and Shepherd, 1997). Optical imaging and other studies have demonstrated that individual glomeruli respond to multiple odorants (Friedrich and Korsching, 1997; Rubin and Katz, 1999; Sachse et al., 1999; Xu et al., 2000, 2003; Meister and Bonhoeffer, 2001; Wachowiak and Cohen, 2001). It is therefore assumed that odorant information is contained in the combination, the relative response intensity, and possibly the spatial position of activated glomeruli. We use the term "map" to encompass all of these response features.

Odorant response maps are most often presented as static entities (Johnson et al., 1998; Wachowiak and Cohen, 2001; Xu et al., 2003), yet temporally dynamic patterns of OB activity have long been thought to play a role in olfactory processing (Adrian, 1950; Meredith, 1986; Wellis et al., 1989; Friedrich and Laurent, 2001; Laurent, 2002). Imaging studies in the OB and the antennal lobe of insects have revealed that spatial activity patterns in the OB change over time during an odor response (Kauer et al., 1987; Cinelli et al., 1995; Sachse and Galizia, 2002; Spors and Grinvald, 2002). The signals measured in these studies reflected predominantly the activity of neurons postsynaptic to sensory afferents. It is therefore not known whether this temporal patterning arises exclusively from circuit interactions, or whether activity patterns across the array of sensory inputs are also dynamic. Partly, this presumption arises from the fact that recordings from single ORNs have reported little temporal structure in odorant responses (Duchamp-Viret et al., 1999; Friedrich and Laurent, 2001; Reisert and Matthews, 2001). *In vivo*, however, multiple factors may influence the temporal structure of primary sensory input to the OB, such as inhalation patterns (sniffing), chromatographic effects in the nasal cavity (Ezeh et al., 1995; Kent et al., 1996), and presynaptic inhibition of ORN axon terminals (Wachowiak et al., 2005).

We therefore directly examined whether odorant response

Received July 27, 2005; revised Nov. 24, 2005; accepted Dec. 13, 2005.

This work was supported by Bundesministerium für Bildung und Forschung, WIN College of the Heidelberg Academy of Science, Max-Planck-Gesellschaft, and National Institutes of Health Grants DC00378, DC04938, and DC05259. We thank the members of the WIN Group of Olfactory Dynamics, the members of the Wachowiak laboratory, Troy Margrie, and Andreas Schaefer for discussions and comments on this manuscript.

* H.S. and M.W. contributed equally to this work.

Correspondence should be addressed to Hartwig Spors, WIN Group of Olfactory Dynamics, Max-Planck-Institut für Medizinische Forschung, Jahnstrasse 29, D-69120 Heidelberg, Germany. E-mail: spors@mpimf-heidelberg.mpg.de.

DOI:10.1523/JNEUROSCI.3100-05.2006

 0270-6474/06/261247-13$15.00/0

maps show temporal complexity at the level of primary afferent input to OB glomeruli by imaging odorant-evoked calcium influx into the presynaptic terminals of ORNs. ORNs were loaded with a calcium-sensitive dye (Friedrich and Korsching, 1997; Wachowiak and Cohen, 2001) and ORN input to individual glomeruli was measured optically in anesthetized mice. We found that the temporal dynamics of these input signals varied across glomeruli in an odorant-specific manner, giving rise to pronounced temporal changes in odorant response maps. Much of these dynamics recurred during each breathing cycle, were consistent across individuals, and occurred during a time window that is relevant for behavioral odorant discrimination (Uchida and Mainen, 2003; Abraham et al., 2004).

Materials and Methods

Animals, dye loading, and preparation. Experiments were performed on 32 C57BL/6 mice (8–12 weeks of age). ORNs were loaded *in vivo* with Calcium Green-1 dextran or Oregon Green 488 BAPTA-1 dextran (10 kDa; Invitrogen, Eugene, OR) as described previously (Friedrich and Korsching, 1997; Wachowiak and Cohen, 2001). Experiments were performed 4–8 d after dye loading under anesthesia with pentobarbital (50 mg/kg, i.p.). Pentobarbital was supplemented during the experiments to maintain a heart rate of 400–500 beats per minute. In most experiments, animals were breathing freely. In some experiments designed to compare temporal response properties of individual glomeruli across animals and to vary the sniff rate, an artificial sniff paradigm was used (Wachowiak and Cohen, 2001). Briefly, a double tracheotomy was performed, and mice respired freely through the lower tracheotomy tube. A stream of pure oxygen was sometimes directed at the lower tracheotomy tube to stabilize the heart rate. Odorant access to the nasal epithelium was controlled by negative square pressure pulses [flow rate, 150 ml/min (or 75 ml/min if one nostril was blocked); 150 ms; 3.3 Hz] applied to the upper tracheotomy tube.

Animals were mounted in a stereotaxic head holder designed not to interfere with respiration. Local anesthetic was applied to all pressure points and incisions. The skin over the dorsal OBs was removed, and the bone was thinned. For use of air objectives, Ringer's solution and a coverslip were placed over the thinned bone. All animal procedures were performed in accordance with official animal care guidelines and approved by the Federal Republic of Germany and by the Yale University and Boston University Animal Care and Use Committees.

Measurement of respiration. In freely breathing animals, respiration was measured as the movement of the thorax by a piezoelectric strap around the animal's chest. During each respiration cycle, one sharp negative deflection in the piezoelectric signal occurred during thorax expansion. The peak of this deflection was used as a time reference for measurements of response latency relative to inspiration. The relationship between this thorax expansion signal and the air flow dynamics in the nose is, however, not known accurately. Hence, the absolute response latency values reported here cannot be interpreted as latencies relative to onset of odorant exposure. This does not affect our analyses because relative response latency measures (see below and Results) were used to allow for the comparison of data across individuals. It is not possible, however, to compare the absolute latency values reported to reaction times in behavioral experiments (Karpov, 1980; Goldberg and Moulton, 1987; Uchida and Mainen, 2003; Abraham et al., 2004).

In artificially sniffing mice, each sniff was controlled by a command pulse. The onset of this command pulse was used as a time reference for the measurements of response latency.

Odorant stimulation. Odorants were applied for 1–4 s using flow dilution olfactometers as described previously (Wachowiak and Cohen, 2001; Spors and Grinvald, 2002; Wachowiak et al., 2004). All olfactometers were based on the design by Kauer and Moulton (1974), used dedicated lines for each odorant to avoid cross-contamination, and allowed for the continuous control of odorant concentration over 1.5–2 log units. These odor concentrations are indicated below as percentage saturated vapor (% s.v.). Briefly, medical-grade air filtered through activated charcoal filters was used to dilute the vapor in the headspace of odorant reservoirs to generate the desired concentration. When concentration changes during the experiment were not required, fixed odorant concentrations were sometimes set by dilution of the pure odorant with mineral oil within reservoirs. These odor concentrations are indicated below as percentage liquid dilution (% l.d.). In the freely breathing experiments, data acquisition was triggered on the respiration cycle. In artificially sniffing animals, odorant presentation was synchronized with the artificial sniff cycle. Interstimulus intervals were at least 60 s to minimize adaptation.

Imaging. Image series of the dorsal OB were acquired with three different systems. (1) A CCD camera with either 80 × 80 or 256 × 256 pixels (NeuroCCD SM or SM256; RedShirtImaging, Fairfield, CT) was connected to a Leitz (Wetzlar, Germany) Ortholux II microscope equipped with a 10×, numerical aperture (NA) 0.2, or a 14×, NA 0.4 air objective. Images were acquired at 100–200 Hz and 14 bits and, in most cases, temporally binned to 25 Hz before storage on disk. The OB was illuminated with a 150 W xenon arc lamp with stabilized power supply (OptiQuip, Highland Mills, NY). The fluorescence filter set used was 480/25 (excitation filter), LP515 (dichroic), and LP530 (emission filter). Excitation light was attenuated by 50–75% with neutral density filters. This system provided fast imaging capabilities, a large field of view, and low noise. (2) A cooled CCD camera (1040 × 1392 pixels; CoolSnapHQ; Photometrics, Tucson, AZ) was attached to a custom-made upright epifluorescence microscope using a BX-RFA epifluorescence condenser (Olympus, Tokyo, Japan) and a 20× water objective (NA 0.95; Olympus) (Wachowiak et al., 2004). The OB was illuminated with a 150 W xenon arc lamp with stabilized power supply (OptiQuip), attenuated to 1.5–25% of the full intensity by neutral density filters. The fluorescence filter set used was 495/30 (excitation filter), LP520 (dichroic), and 545/50 (emission filter). Images were spatially binned 4 × 4 or 8 × 8 and digitized at 12 bits and 10–45 Hz. This system provided a high signal-to-noise ratio, high spatial resolution, and low bleaching rate but a relatively small field of view. (3) Images were acquired using a CMOS camera (128 × 128 pixels; HR Deltatron 1700; Fuji, Tokyo, Japan) and a tandem photo lens system (NA 0.46; Navitar 25 mm, $f = 0.95$; and Nikkor 135 mm, $f = 2$) (Spors and Grinvald, 2002) at 14 Hz. The OB was illuminated using a 100 W halogen lamp, a stabilized power supply (Kepco, Flushing, NY) and filters 480/40 (exciter), LP 505 (dichroic), and 535/50 (emission filter). This system provided intermediate temporal and spatial resolution and a large field of view.

Raw images were converted to images representing the relative change in fluorescence ($\Delta F/F$) in each pixel and frame after stimulus application. The baseline fluorescence (F) was calculated by averaging frames over 0.5–1 s before stimulus onset. Data taken with systems 1 and 3 were corrected for bleaching by subtracting $\Delta F/F$ image series without odorant stimulation. Data taken with system 2 were not bleach-corrected because bleaching was minimal owing to the strong attenuation of the excitation light. Data analysis was performed using NeuroPlex software (RedShirtImaging), and routines were written in Igor Pro and Matlab. For display purposes only (not for analysis), the resolution of images obtained with system 1 was increased from 80 × 80 to 160 × 160 pixels by linear interpolation. No temporal filters were applied unless stated otherwise.

Data analysis. In different freely breathing animals, the trigger of the odorant stimulus could occur at slightly different phases of the breathing cycle, thus complicating the comparison of absolute response latencies across animals. We therefore used relative response latencies in most analyses. To calculate these, latencies were measured from the first inspiration trigger pulse after onset of stimulation in each animal. Relative latencies were then calculated by subtracting the mean response latency, averaged over all glomeruli, in each trial.

Focal changes in $\Delta F/F$ in the OB have been shown previously to correspond to individual glomeruli (Belluscio and Katz, 2001; Meister and Bonhoeffer, 2001; Wachowiak et al., 2004). Glomeruli were either selected manually by outlining spatially discrete $\Delta F/F$ signals matching the size of a glomerulus, or by a semiautomated procedure. In this procedure, maps integrated over the first respiration cycle were spatially bandpass filtered using two Gaussian kernels (low pass: $\sigma = 25$ μm; high pass:

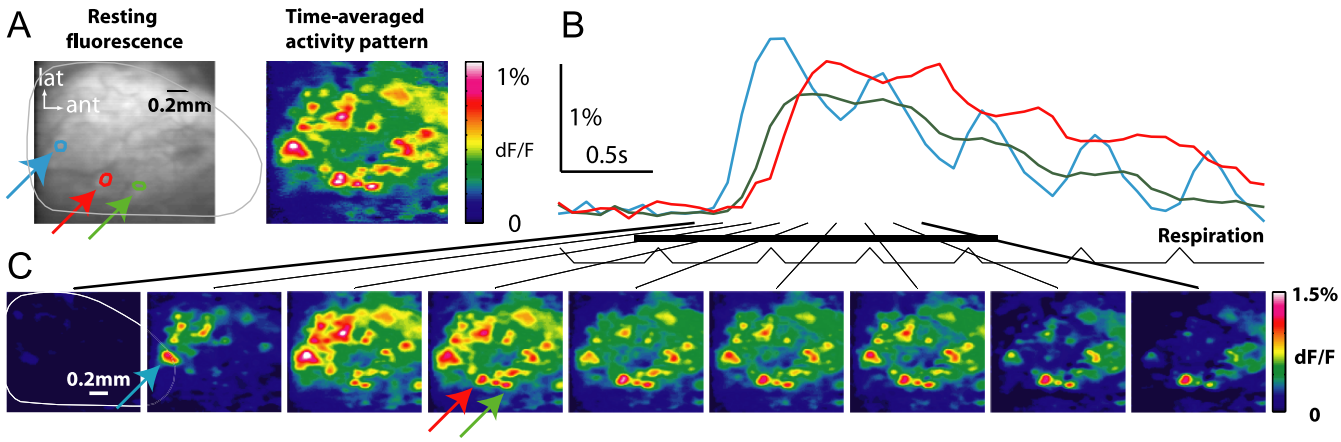

Figure 1. Spatiotemporal patterning of sensory input to the olfactory bulb. ***A***, Left, Fluorescence image of the dorsal OB after loading of ORN axons with Calcium Green-1 dextran. The outline of the dorsal OB is shown in gray. Right, Relative change in fluorescence in the same view evoked by ethyl butyrate (1% s.v.), averaged over the first respiration cycle. lat, Lateral; ant, anterior. ***B***, Response time course of three glomeruli (see arrows with corresponding colors in ***A*** and ***C***). The black bar indicates the odorant valve opening. Peaks in respiration trace do not correspond to the beginning of inspiration (see Materials and Methods). ***C***, Patterns of fluorescence signals in successive 154 ms time windows (averages of 2 frames) centered on the time points indicated by the lines. The arrows point to the glomeruli depicted in ***B***.

$\sigma = 300\ \mu$m) to enhance contrast (Meister and Bonhoeffer, 2001; Spors and Grinvald, 2002; Wachowiak and Cohen, 2003). Local maxima were determined in these maps. Pixels within a distance of $<25\ \mu$m from the local maxima were labeled and averaged. All automatically determined glomeruli were visually inspected, and overlapping glomeruli were discarded.

In freely breathing mice, image acquisition was triggered on respiration pulses (see above) or traces from freely breathing mice were aligned on the first peak in the respiration trace (see above) during the odor response. Because of slightly varying respiration frequencies, the alignment of later respiration cycles is not as good as for the first inspiration cycle (see Figs. 2*C*, 5*A*).

Latency and amplitude of odorant responses were quantified from sigmoids fitted to the time course of the Ca signal, averaged over all pixels of a selected glomerulus, and cut after the peak of the response to the first inspiration. When fits did not converge because of an insufficient signal-to-noise ratio, data were excluded from the analysis. Response amplitude was given by the maximum of the sigmoid fit. Response latency was determined as the time to 10% or 50% amplitude of the sigmoid (t_{10} and t_{50}, respectively).

Time shifts between glomerular responses in an activity map were calculated as in Spors and Grinvald (2002). Briefly, data were filtered in time 1 Hz below and 1 Hz above the respiration frequency (sixth-order Butterworth filter). Responses were then averaged over all selected glomeruli. The time course of this averaged signal was cross-correlated with the time course in each glomerulus. The offset of the peak in the cross-correlogram from $t = 0$ was taken as the time shift measure. To increase the resolution of the shift analysis, the temporal resolution of the data was increased by low-pass interpolation (Digital Signal Processing Committee, 1979), or the shift of the peak in the cross-correlogram was determined by fitting a second-order polynomial.

The respiration modulation was defined as the amplitude of respiration-modulated calcium signal, relative to the tonic component of the calcium signal. The amplitude of the respiration-modulated signals was determined as the peak of the amplitude spectrum at respiration frequency. The tonic component was determined as the calcium signal amplitude after low-pass filtering at 1 Hz. The respiration modulation is given by the ratio of these values.

The change of the glomerular response map over time was calculated by pairwise correlation of vectors consisting of the response amplitudes of all activated glomeruli in a given time window. This correlation was calculated for all possible combinations of time windows within one respiration cycle. Signal-to-noise ratio was improved by averaging one-half of the available repetitions of the same odorant before correlation. Signal-to-noise ratio and variability across trials was assessed by again randomly pooling all available odorant repetitions into two groups, averaging responses within each group, and correlating the response vectors from each group at corresponding time points. These calculations were repeated for all combinations of the repetitions.

In most glomeruli, responses were largest shortly after response onset and decreased subsequently. The decrease in signal amplitude over time may be attributable to adaptation of olfactory receptor neurons and, at later times, reflect the contribution of an intrinsic signal. At the excitation and emission wavelengths used here, the measured change in intrinsic fluorescence is spatially diffuse and not modulated at the respiration frequency. It starts ~500 ms after response onset and develops more slowly than the Ca signal (Bozza et al., 2004; H. Spors and R. W. Friedrich, unpublished results), thus affecting only later phases of the response. No attempt was made to correct for the intrinsic signal because our analysis focused primarily on the initial phase of the response, when the contribution of the intrinsic signal is minimal, or examined temporal features in frequency bands in which the intrinsic signal has little power (Spors and Grinvald, 2002; Wachowiak and Cohen, 2003).

Statistical comparisons were performed by a Wilcoxon rank–sum test unless stated otherwise.

Results

Patterns of glomerular activation are dynamic

We measured odorant-evoked patterns of ORN input to glomeruli in the dorsal OB of mice after loading ORNs with Calcium Green-1 dextran as described previously (Friedrich and Korsching, 1997; Wachowiak and Cohen, 2001; Fried et al., 2002; Wachowiak et al., 2004). Odorant stimulation evoked fluorescence changes reflecting calcium influx into ORN presynaptic terminals in discrete foci corresponding, most likely, to individual glomeruli (Belluscio and Katz, 2001; Wachowiak et al., 2004). Spatial maps of this glomerular input signal, generated by averaging fluorescence signals over the first respiration cycle, were odorant specific and often distributed across many glomeruli (Fig. 1*A*), as reported previously (Wachowiak and Cohen, 2001; Fried et al., 2002; Bozza et al., 2004).

We found that the time courses of the glomerular calcium signals varied between glomeruli activated by the same odorant (Fig. 1*B*). Temporal parameters that differed across glomeruli included the latency to response onset, the rise time of the response, and the extent to which the evoked signal was modulated by respiration (sniffing). Changes in response maps were apparent both within a breathing cycle and across subsequent cycles. As

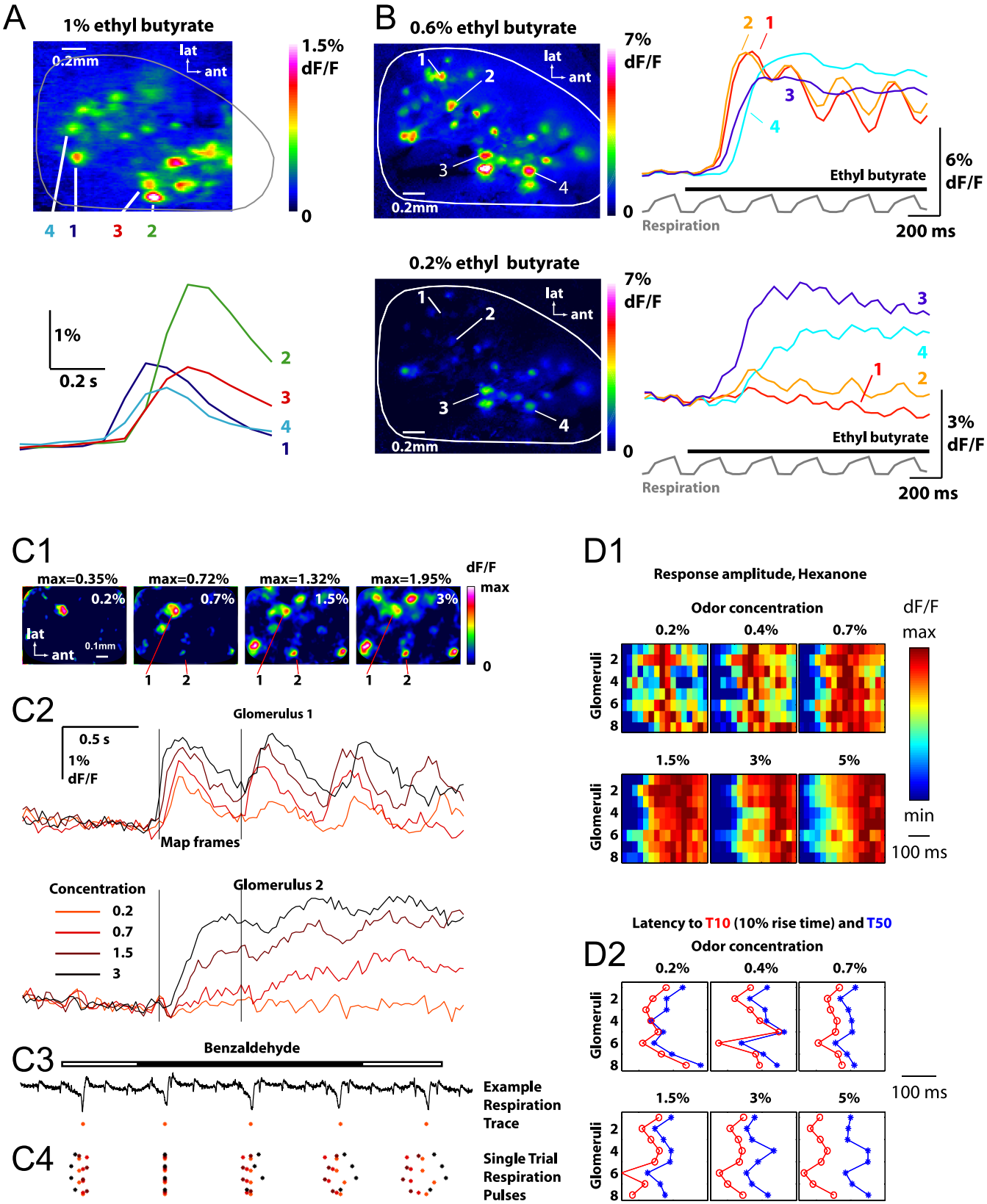

Figure 2. Temporal response diversity in individual glomeruli. ***A***, Response latency, rise time, and amplitude can vary independently. Top, Response map evoked by ethyl butyrate (1% l.d.), averaged over the first respiration cycle. Bottom, Time course of the calcium signals in four glomeruli (locations shown in map) during the first respiration cycle. Average of four repetitions triggered on respiration. ***B***, Odorant sensitivity and response latency can vary independently. Left, Maps averaged over 1 s in response to 0.2 and 0.6% s.v. ethyl butyrate. Glomerulus 1 does not respond at the lower concentration. Right, Time courses of four selected glomeruli at both concentrations. The less sensitive glomerulus 1 responds with shorter latency at the higher (*Figure legend continues*.)

a consequence, maps of ORN input to glomeruli of the dorsal OB changed throughout the odorant response (Fig. 1*C*).

Temporal dynamics of glomerular responses: qualitative observations

As illustrated in Figure 2*A*, glomeruli activated by the same odorant could respond with different latencies, rise times, and amplitudes. In isolated sensory neurons, these response parameters are often correlated: with increasing stimulus strength, response amplitudes increase and response latency and rise time decrease (Firestein et al., 1993; Reisert and Matthews, 2001). In glomeruli *in vivo*, however, these response parameters appeared to be only weakly correlated, as illustrated in the example in Figure 2*A*: glomeruli 1 and 3 responded with different latencies but with similar rise times and amplitudes; glomeruli 2 and 3 responded with similar latencies but with different amplitudes.

We also observed that glomeruli responding with the shortest latencies to a given odorant were not necessarily the ones that were the most sensitive to that odorant. For example, in Figure 2*B*, glomeruli 1 and 2 responded with shorter latencies than glomeruli 3 and 4 to ethyl butyrate at a concentration of 0.6% s.v. (saturated vapor). At 0.2% s.v., however, glomeruli 1 and 2 responded weakly or not at all, whereas glomeruli 3 and 4 still responded strongly. Hence, glomeruli 1 and 2 were less sensitive to ethyl butyrate than glomeruli 3 and 4 but responded faster. This result suggests that response latency is not solely determined by odorant/receptor affinity.

Glomerular responses were often modulated by respiration, with a phasic component of the response appearing after each inhalation. The magnitude of this modulation varied markedly across glomeruli. For example, the blue glomerulus in Figure 1*B* showed pronounced phasic responses with each inhalation, whereas the red and green glomeruli responded more tonically. Glomeruli whose responses were strongly modulated by respiration tended to have shorter response latencies than glomeruli showing little or no modulation ($r = -0.48 \pm 0.04$; quantified in three animals, 71 glomeruli, responses to ethyl butyrate). For example, Figure 2*C* shows responses of two glomeruli to different concentrations of benzaldehyde. The response of glomerulus 1 was strongly modulated by respiration at all concentrations, whereas the response of glomerulus 2 was only weakly modulated. At all concentrations, the response latency of glomerulus 1 was clearly shorter than that of glomerulus 2. Figure 2*C* (glomerulus 2) also shows that the absence of breathing-related modulation is not attributable to saturation of the calcium indicator, because modulation was also absent in response to subsaturating stimuli. An example of a respiration trace (Fig. 2*C3*) and the individual respiration cycles are indicated below the imaging traces (Fig. 2*C4*) (see Materials and Methods for alignment procedure). In some glomeruli, rise times were slow enough that the onset phase of the odorant-evoked response spanned multiple respiration cycles (Fig. 2*C*, glomerulus 2, 0.7% s.v.). As a result, maps of glomerular input could change during the course of a single respiratory cycle as well as over the course of multiple cycles.

With increasing odorant concentration, response amplitudes of individual glomeruli increased and additional glomeruli were recruited, as described previously (Stewart et al., 1979; Guthrie et al., 1993; Friedrich and Korsching, 1997; Meister and Bonhoeffer, 2001; Wachowiak and Cohen, 2001; Fried et al., 2002; Spors and Grinvald, 2002; Wachowiak et al., 2004). At the highest concentrations tested, the rising phase of some responses consisted of the initial steep increase in $\Delta F/F$, followed by a slower and smaller increase that was not observed at lower concentrations (Fig. 2*C2*, glomerulus 1). Moreover, response latencies often decreased slightly with increasing stimulus concentration, as shown in Figure 2*C*. This was observed independently of the extent to which responses were modulated by breathing (Fig. 2*C*). As a result, the dynamics of the activity pattern across glomeruli responding to a given stimulus over a certain concentration range was similar at different concentrations. In Figure 2*D*, the initial time-varying activity pattern across eight glomeruli responding to 2-hexanone at six different concentrations is represented by color raster plots. The pattern of response latencies across the eight glomeruli at each concentration is depicted by line profiles. Latency patterns remained similar, albeit not identical, over the concentration range tested. Increasing stimulus concentrations also recruited additional glomeruli, some of which responded with short latencies (Fig. 2*B*). Patterns of response latencies across all glomeruli therefore change with concentration, but patterns of relative response latency across subsets of glomeruli are partially preserved within a certain concentration range.

Quantitative analysis of temporal response parameters

To generate a more quantitative description of glomerular response dynamics, we measured the amplitude, latency, and rise time of the presynaptic calcium signal by fitting sigmoid curves to the optical signal just after stimulus onset (Fig. 3*A*). Response amplitude was measured as the maximum of the fit (E_{max}); rise time was measured as the time between 10 and 90% of the maximum ($t_{90} - t_{10}$); and latency was measured as the time from the first respiration cycle after odorant onset to 50% of the maximum (t_{50}). Measuring latency as the time to 10% of the maximum (t_{10}) was less robust to noise but produced similar results (data not shown). Because the effective odorant onset and sniff onset were not determined in absolute time values, relative response latencies were calculated for each glomerulus by subtracting the mean latency of all fitted glomeruli during the same stimulus presentation (see Materials and Methods).

To statistically characterize responses of many glomeruli to different odorants, three anesthetized, freely breathing mice were each stimulated with three different odorants (ethyl butyrate, 1% s.v.; benzaldehyde, 3% s.v.; and 2-hexanone, 3% s.v.). Temporal response parameters were quantified in a total of 335 glomeruli,

←

(*Figure legend continued*.) concentration. Maps and traces are averaged over four odorant presentations. Traces were low-pass filtered at 5 Hz with a Gaussian kernel. Maps were smoothed slightly by increasing the pixel resolution by a factor of 2 and interpolating between pixels. Mice were artificially sniffing. The gray traces show suction applied to the upper tracheotomy tube. The upward deflection corresponds to inspiration. ***C1***, Time- averaged maps of responses to four different concentrations of benzaldehyde. Response amplitudes increase and additional glomeruli are recruited with increasing concentration. ***C2***, Time course of the calcium signal from two glomeruli in response to the four different odorant concentrations. Each trace is averaged over four repetitions. Because of differences in breathing rate from trial to trial, the peaks occur at different times. The differences in respiration timing for the four trials shown are illustrated in ***C4***. ***C3***, An example of a respiration trace and time points of peaks (dots) in the respiration trace. ***C4***, Time points of respiration trace peaks from all traces averaged and displayed in ***C2*** (same colors). The traces were aligned to minimize time shift at the beginning of the odorant response. ***D1***, Color-coded time course of calcium signals evoked by 2-hexanone at six different concentrations in eight glomeruli (different preparation than in ***C***). Each column is a different time window (26 ms), and each row corresponds to an individual glomerulus. The response is normalized to the maximum for each glomerulus. ***D2***, Latency profile from the same concentrations as in ***D1***, measured as the time to half-maximum (T50, blue) or time to 10% of the maximum (T10, red). lat, Lateral; ant, anterior.

all of which responded to at least one of the test odorants. The respiration rate in these mice ranged between 1.5 and 2 Hz. The mean (median) amplitude, $\Delta F/F$, of the response was 1% (0.9%) ± 0.6% (SD). The mean (median) rise time of the calcium signal was 143 (135) ± 99 ms (SD). The SD of the response latency was 48 ms. The SD values of these response parameters reflect both inherent differences in the temporal pattern of input to different glomeruli, as well as trial-to-trial variability of response dynamics (see below).

We next determined whether different response parameters were correlated to each other, which would indicate that they reflect similar stimulus properties. Response latency and rise time were positively correlated for all three odorants tested (Table 1). Response amplitude and rise time were positively correlated for two of the three tested odorants. Response latency and amplitude were positively correlated in response to one odorant, not significantly correlated in response to the second odorant, and negatively correlated in response to the third odorant (Table 1). For all three odorants, the positive or negative correlation between latency and amplitude was weak ($r^2 = 0.012$, 0.003, and 0.034 for ethyl butyrate, benzaldehyde, and 2-hexanone, respectively). Hence, consistent with our qualitative observations (Fig. 2*A*), no consistent relationship between response latency and amplitude was observed. Thus, each of these two parameters could carry distinct information about a stimulus (Optican and Richmond, 1987).

We then focused on response latencies in more detail, because they can provide stimulus information in other sensory systems (Gawne et al., 1996; Richmond et al., 1997) and because measurements of response latency are minimally confounded by the decay kinetics of the calcium signal or by the slower, superimposed intrinsic signal. To facilitate the comparison of response latencies across animals, we measured a relative response latency value for each glomerulus, calculated as the absolute response latency for a glomerulus minus the mean latency for all glomeruli in a given trial.

We first assessed the trial-to-trial variability of glomerular response latencies using repeated applications of the same odorant. Data were obtained from 174 glomeruli ($n = 8$ mice) responsive to ethyl butyrate (1% s.v. or l.d.), from 59 glomeruli ($n = 3$ mice) responsive to benzaldehyde (3% s.v.), and from 93 glomeruli ($n = 3$ mice) responsive to 2-hexanone (3% s.v.). For each glomerulus, the average of the relative response latencies across repeated trials (eight for ethyl butyrate; four for benzaldehyde and 2-hexanone) was subtracted from the relative latency measured in each trial, thereby centering the distribution of latency values for each glomerulus on zero. Distributions of response latencies were then pooled across all glomeruli. The pooled distributions had a Gaussian-like shape. The SDs of the pooled distributions are a measure of the average trial-to-trial variability of response latencies and were 23, 16.8, and 19.9 ms for stimulation with ethyl butyrate, benzaldehyde, and 2-hexanone, respectively (Fig. 3*B–D*, gray histograms).

To compare response latencies across glomeruli, relative latency values were not centered on zero by subtraction of the glomerulus-specific mean latency before pooling. The resulting distributions therefore reflect the differences in response latencies between glomeruli. These distributions were significantly broader than the trial-to-trial variability of glomerular response latencies (Fig. 3*B–D*, black histograms) (ethyl butyrate: SD, 51 ms; benzaldehyde: SD, 45.5 ms; 2-hexanone: SD, 39.4 ms; $p <$ 0.001 in all cases, Kolmogorov–Smirnov test). Thus, significant differences exist between the response latencies of different glomeruli to the same odorant. Eighty percent of this variation falls

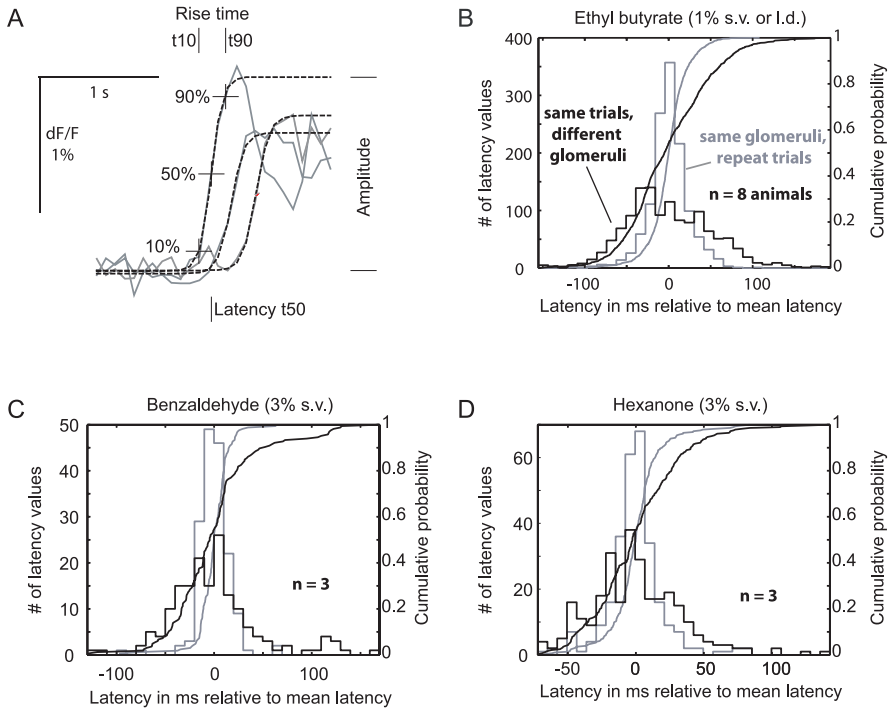

Figure 3. Variation of response latency. ***A***, Examples of sigmoid fits overlaid onto the onset of the fluorescence signal for three glomeruli responding to ethyl butyrate (1% l.d.). The quantified parameters are indicated in the plot. ***B–D***, Distributions of relative response latencies for three different odorants, measured in multiple glomeruli from multiple animals (see Results). The *y*-axis of the histograms (left side) indicates the number of occurrences in each 10 ms time bin. Gray histograms, Latency values of each glomerulus were centered on zero by subtracting the glomerulus-specific mean latency (see Results). The distribution reflects trial-to-trial variability of response latency. Black histogram, Distributions of relative response latencies were not centered. This distribution reflects glomerulus-specific differences in response latency. Curves, Cumulative probability distributions of histograms with the same color. ***B***, SD of trial-to-trial variability, 23 ms; SD of glomerulus-specific variability, 51 ms; $p < 0.001$, Kolmogorov–Smirnov test; data from 174 glomeruli ($n = 8$ mice). ***C***, SD of trial-to-trial variability, 16.8 ms; SD of glomerulus-specific variability, 45.5 ms; $p < 0.001$, Kolmogorov–Smirnov test; data from 59 glomeruli ($n = 3$ mice). ***D***, SD of trial-to-trial variability, 19.9 ms; SD of glomerulus-specific variability, 39.4 ms; $p < 0.001$, Kolmogorov–Smirnov test; data from 93 glomeruli ($n = 3$ mice).

Table 1. Correlations between response amplitude and temporal response parameters of glomerular inputs

	Amplitude versus latency	Amplitude versus rise time	Rise time versus latency
Ethyl butyrate (183 glomeruli, 8 mice, 64 trials)	0.109**	0.217**	0.100**
Benzaldehyde (59 glomeruli, 3 mice, 12 trials)	−0.054	0.272**	0.370**
2-Hexanone (93 glomeruli, 3 mice, 10 trials)	−0.184**	0.011	0.405**

Data were obtained from multiple glomeruli in different animals as indicated. Latencies were calculated as relative latencies (see Materials and Methods). Values given are Pearson correlation coefficients. Significant correlations are indicated by asterisks (**$p < 0.01$).

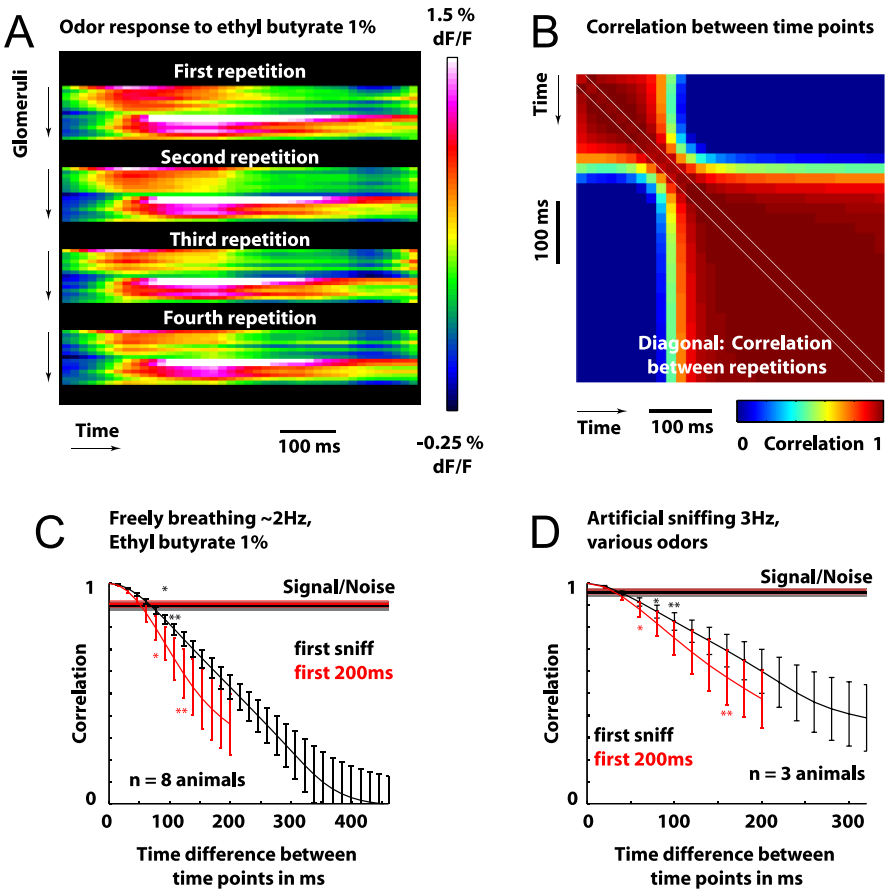

Figure 4. Change of glomerular response maps during a respiration cycle. ***A***, Responses of 15 glomeruli to four presentations of ethyl butyrate (1% l.d.). Each row corresponds to one glomerulus. The *x*-axis represents time. ***B***, Correlation of response pattern between different time points. The *x*- and *y*-axes both represent time. Each pixel corresponds to the correlation value between patterns at the time points of the *x*- and *y*-axes. Displayed is the average correlation generated from eight repetitions of the odorant ethyl butyrate (1% l.d.) in the same animal (see Materials and Methods). The correlation coefficient is color coded. The diagonal shows the correlation between repetitions (measure of signal-to-noise ratio) instead of the autocorrelation. ***C***, Correlation between time points as a function of the time difference (Δt) between them. The black curve represents the first sniff cycle. The red curve represents the first 200 ms. The horizontal bars indicate the correlation between repetitions (measure of signal-to-noise ratio). The error bars are SEM calculated over eight animals after averaging the values from data with eight repetitions of the odorant presentation. Significance levels: $*p < 0.05$; $**p < 0.01$. ***D***, Same analysis for responses in mice artificially sniffing at 3 Hz. Odorants were ethyl butyrate (3 animals); methyl benzoate (2 animals); hexanal and heptanone (1 animal each). Odorant presentations were repeated three or four times.

within a range of 127, 98, and 84 ms for the odorants ethyl butyrate, benzaldehyde, and 2-hexanone, respectively.

We next measured the extent to which glomerular response maps change within one respiration cycle. First, to assess the reproducibility of responses, we compared spatiotemporal glomerular response patterns within the first respiration cycle between repetitions of the same stimulus. Figure 4*A* shows time courses of fluorescence signals in 15 glomeruli in response to repeated stimulation with ethyl butyrate in a freely breathing animal. Second, the similarity of response patterns across the 15 glomeruli in different time windows of the same trials was measured by the correlation coefficient, resulting in a correlation matrix in which the two axes represent time (Fig. 4*B*). The autocorrelations with zero time shift have been replaced by the average cross-correlation of repeated responses to the same odor. The correlation coefficients along the diagonal therefore represent the similarity of response maps evoked by repeated stimulation within the same time window, whereas off-diagonal values represent the similarity between responses in different time windows of the same trials. The similarity of response patterns relative to a certain time window is given by rows or columns of this correlation matrix.

To quantify the rate of change of response patterns, correlation matrices as in Figure 4*B* were obtained for responses to ethyl butyrate in eight freely breathing animals. For each time window, the similarity of the response pattern to patterns in all other time windows was quantified. Figure 4*C* shows the average similarity between activity patterns as a function of time difference (i.e., the correlation is the average for all time-differences of a certain amount over the sniff, as opposed to correlating one point with another fixed reference time point). Correlation decreased with increasing time difference, indicating that glomerular response patterns change substantially within a single respiration cycle. To verify that this change is not attributable to measurement noise or response variability across trials, we also computed the average correlation between response maps evoked by repeated stimulation within the same time window from the diagonals of the correlation matrices. Throughout the respiration cycle, this correlation was >0.9 (Fig. 4*C*), indicating that the observed changes in glomerular response patterns cannot be explained by variability attributable to noise. The rate of change of response patterns was not equal throughout the respiration cycle, but the fastest changes were usually observed within the first 200 ms after response onset (Fig. 4*B*,*C*). Similar results were obtained in tracheotomized animals artificially sniffing at 3 Hz in response to various odorants (three animals; four odorants) (Fig. 4*D*). Hence, glomerular response patterns change significantly during a single respiration cycle ($p < 0.05$ after 60–100 ms; one-tailed *t* test).

Odorant specificity of map dynamics

Temporal patterns of ORN inputs to different glomeruli were odorant specific. Figure 5*A* shows response time courses of five individual glomeruli to three different odorants. Each trace was normalized to its peak amplitude. The time-averaged glomerular activation maps evoked by these odorants overlapped substantially, so that several glomeruli were activated by all three stimuli (Fig. 5*B*). For any one glomerulus, however, different odorants could evoke responses with different latencies. For example, glomerulus 1 was activated with the shortest latency by ethyl butyrate, with a longer latency by octanal, and with a still longer latency by hexyl acetate (Fig. 5*A*,*C*). The response latencies of these glomeruli from four repeated trials with each odorant are plotted in Figure 5*D*. Glomerulus 1 (blue) responded before glomerulus 4 (cyan) to ethyl butyrate but after glomerulus 4 to octanal. Additional examples of odorant-specific latency patterns across glomeruli are shown in Figure 5*E*. Hence, the pattern of

response latencies across glomeruli, and therefore the sequence of glomerular activation across the dorsal OB, was odorant specific ($p < 0.001$ in all cases, both using two-way ANOVA or Friedman's nonparametric two-way ANOVA). Other temporal response parameters also depended on the odorant. For example, a glomerulus could respond to one odorant with strong modulation by the respiratory cycle, and respond to a different odorant with little or no modulation (Fig. 5*A*, glomeruli 2, 3), despite showing similar response amplitudes.

These observations show that the time courses of glomerular responses depend on both the ORNs innervating a glomerulus and the odorants that activate them. Moreover, the dynamics of odorant-evoked glomerular activation maps cannot be explained by artifacts of dye loading or preparation health, because they should affect the response to all odorants equally. Odorant-specific information may therefore be carried not only by the combination of activated glomeruli, but also in the temporal dynamics of their activation.

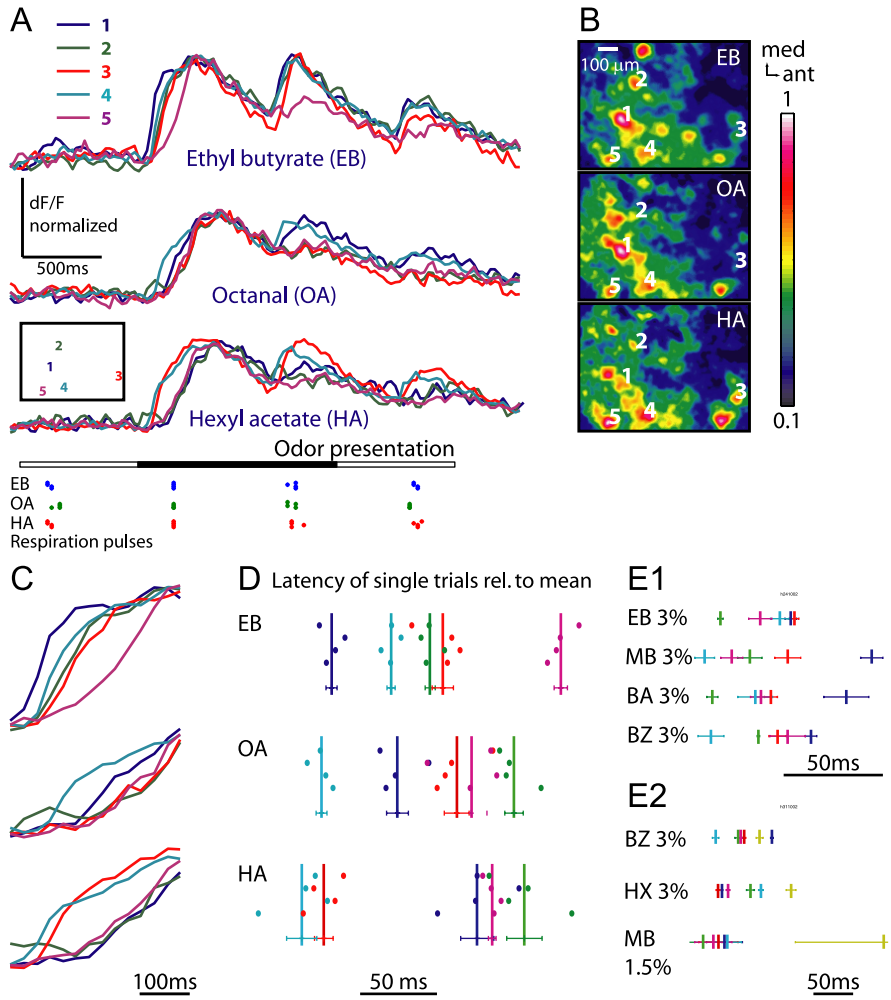

Figure 5. Odorant-specific patterns of response latency across glomeruli. ***A***, Response time courses of five glomeruli to each of three odorants (5% s.v.), normalized to the maximum for each response. Average of four repetitions. For location of the glomeruli, see ***B***. Odor stimulation and respiration pulse are shown as in Figure 2*C*. ***B***, Spatial activity patterns evoked by the three different odorants, averaged in time over the first respiration cycle, normalized to their maximum. Average of four odorant presentations. med, Medial; ant, anterior. ***C***, Enlargement of the time courses in ***A*** during response onset. The trace colors are as in ***A***. ***D***, Response latencies of each glomerulus to four repetitions of each stimulus. Each dot depicts the relative response latency of one glomerulus in one trial, measured as the time to half-maximum of a sigmoid fit to the response onset (Fig. 3*A*). The horizontal error bars depict mean and SEM of latencies for each glomerulus and odorant. The colors of plot symbols correspond to trace colors in ***A***. ***E1***, ***E2***, Two additional examples for odorant-specific latencies from two different animals using the same conventions as in ***D***. MB, Methyl benzoate; BA, butyl acetate; BZ, benzaldehyde; HX, 2-hexanone. The colors in the same panel represent the same glomerulus. The colors in different panels do not depict corresponding glomeruli.

Activity pattern dynamics across respiration cycles

During prolonged odorant exposure, an animal repeatedly samples a stimulus. Most glomeruli responded to an odorant with calcium transients during each inhalation cycle. We therefore asked whether the dynamics of glomerular response patterns during subsequent breathing cycles in a single odorant presentation are related. Figure 6*A* shows a series of response maps, each integrated over 77 ms, during the first three respiration cycles after stimulation with 1% l.d. ethyl butyrate. The spatial map of activated glomeruli changed markedly during the first respiration cycle after stimulus onset, as described above. In particular, an anterior–medial group of glomeruli responded significantly later than a group of caudal–lateral glomeruli. In the following respiration cycles (Fig. 6*A*, rows 2 and 3), the sequence of changes in the response maps was similar to that during the first cycle. Consistent with these observations, timing differences were observed between calcium transients from different glomeruli and persisted across breathing cycles (Fig. 6*B*).

To further investigate the dynamics of response maps across respiration cycles, a series of activity maps was separated into segments corresponding to individual cycles. Within each segment, the time shift between the response time course of single glomeruli and the average response were determined by cross-correlation (Spors and Grinvald, 2002) (see Materials and Methods). The resulting maps of relative response times were similar to maps of relative response latencies calculated by fitting the sigmoids to the initial response (see Materials and Methods) ($r = 0.97$) (Fig. 6*C*,*D*). During the subsequent respiration cycles, time shift maps remained similar to that of the first breathing cycles (Fig. 6*D*, $r = 0.92$). Glomeruli with large time shifts in the first cycle also exhibited large time shifts in subsequent cycles. Similar results were obtained in six experiments with ethyl butyrate ($r = 0.88 \pm 0.04$; mean ± SEM, correlation across on average 25.8 glomeruli and 3.2 respiration cycles), and for other odorants (e.g., methyl benzoate). Hence, the temporal evolution of maps of glomerular input recurs in a similar, albeit not identical, manner during each respiration cycle in anesthetized animals.

In awake animals, olfactory sampling behavior ("sniffing") varies with the behavioral state and with stimulus strength (Youngentob et al., 1987; Johnson et al., 2003). Respiration frequency increases from 2–3 Hz at rest to 8–10 Hz when the animal actively explores its environment (Youngentob et al., 1987; Kay and Laurent, 1999). To assess the effects of sniff frequency on the dynamics of glomerular response maps, we used an artificial sniff

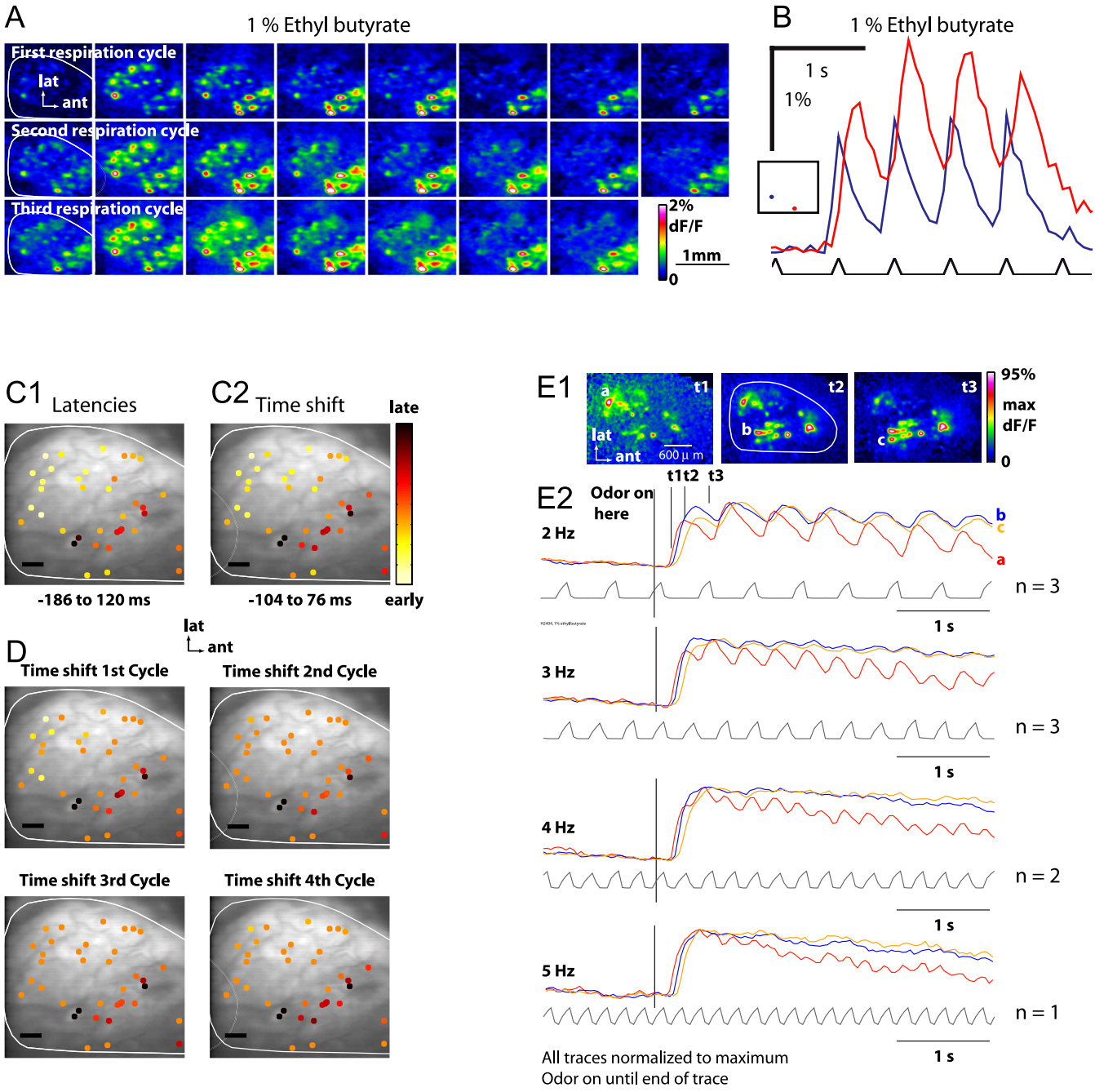

Figure 6. Recurrence of glomerular input pattern dynamics in subsequent breathing cycles. ***A***, Responses across several breathing cycles during stimulation with ethyl butyrate (1% l.d.). Response displayed in movie frames (77 ms) were aligned to respiration and spatially low-pass filtered with a Gaussian kernel ($\sigma = 13.3$ μm). ***B***, Response time courses of two selected glomeruli. ***C1***, Spatial pattern of response latencies for individual glomeruli, measured as time to half-maximum of a sigmoid fit to the response onset (Fig. 3*A*). Regions were selected by an automated procedure detecting glomerular activity structures (see Materials and Methods). ***C2***, Spatial pattern of time shifts of the calcium signal, relative to the mean signal, determined from the response time course over all four breathing cycles. Correlation between ***C1*** and ***C2***, $r = 0.97$. ***D***, Spatial pattern of time shifts of the calcium signal, relative to the mean signal, during subsequent breathing cycles. The color scale and clipping range are as in ***C2***. Average correlation between cycles, $r = 0.94$. ***E***, Effect of increasing respiration frequency in an artificially sniffing mouse. ***E1***, Maps at the time points indicated in the top trace of (***E2***) were integrated over 40 ms, spatially filtered with a Gaussian kernel ($\sigma = 6.5$ μm), and normalized to their maximum. ***E2***, Responses of three glomeruli to the same odorant; suction to the tracheotomy tube was applied at different frequencies. The black trace represents negative pressure in the suction line attached to the upper tracheotomy tube. All traces are scaled to their maximum. *n* indicates number of repetitions averaged for each trace. lat, Lateral; ant, anterior.

paradigm (Wachowiak and Cohen, 2001) and varied sniff frequency from 2 to 5 Hz (Fig. 6*E*). At 2 Hz, glomerular responses showed onset latency differences, sniff-related modulation of response amplitude, and persistent time shifts between responses of different glomeruli, similar to responses in freely breathing animals (Fig. 6*E*). Also consistent with data from freely breathing animals, short response latencies were observed in several caudal–lateral glomeruli, whereas rostral–medial glomeruli responded with longer latencies (Fig. 6*E*) (see below). As sniff frequency was increased, however, the extent of amplitude modulation by the sniff cycle decreased. Typically, those glomeruli with the longest response latencies showed less sniff-driven modulation and showed no modulation at sniff frequencies ≥4 Hz. Sniff-driven modulation persisted in glomeruli with short

response latencies, but the amplitude of modulation was reduced. At 5 Hz, few glomeruli showed modulation by individual sniffs (Fig. 6*E*). Nevertheless, the relative latencies at response onset were not affected by sniffing frequency (Fig. 6*E*). Thus, the particular odorant-specific sequence of activation of different glomeruli evoked by the onset of odorant stimulation persists across a range of sniff frequencies.

Consistency of temporal response patterns across animals

Glomeruli receiving input from ORNs expressing the same odorant receptor are found at similar, albeit not identical, coordinates in the OBs of different individuals (Ressler et al., 1994; Vassar et al., 1994; Strotmann et al., 2000) and have comparable response specificities to different odorants (Wachowiak and Cohen, 2001; Bozza et al., 2002). We therefore examined whether equivalent regions and equivalent glomeruli in different animals respond to odorants with similar response latencies. On a coarse spatial scale, maps of response latency evoked by ethyl butyrate appeared to be regionally organized: glomeruli in the caudal–lateral OB showed shorter-latency responses than glomeruli in the anteromedial OB (Fig. 7*A*,*B*) (see also Figs. 1, 2, 6). This regionalization was observed both in freely breathing (Fig. 7*A*, $n = 6$) and artificially sniffing (Fig. 7*B*, $n = 3$) mice.

In mice, particular glomeruli in the dorsal OB can be tentatively identified across animals based on their location and their high sensitivity to one or a few diagnostic odorants (Wachowiak and Cohen, 2001). As an example, Figure 7*C* shows the positions of glomerulus D [following the convention of Wachowiak and Cohen (2001)] in four animals. No temporal response characteristics were used for this identification. We could therefore ask whether functionally analogous glomeruli in different animals have similar temporal response properties. To minimize breathing-related variability between animals, experiments were performed using the artificial sniff paradigm at 3.3 Hz, response time courses were temporally low-pass filtered (Gaussian filter at 1 Hz), and only response latencies were measured. We first focused on glomeruli D and E, because they have overlapping but distinct odorant response profiles. In animals in which both glomeruli were imaged ($n = 4$), the response of glomerulus D to benzaldehyde was always markedly faster than the response of glomerulus E (Fig. 7*C*). The longer latency and slower rise time of glomerulus E to benzaldehyde was odorant specific: hexanal and isovaleric acid, presented at similar vapor dilutions and eliciting a similar-amplitude response, evoked signals in glomerulus E that had a shorter latency and rise time.

We further examined the response time courses of glomeruli D and E, and an additional identified glomerulus [glomerulus B from Wachowiak and Cohen (2001)] to different odorants in different animals. For each glomerulus, response latencies were compared with the response latency for the reference odorant

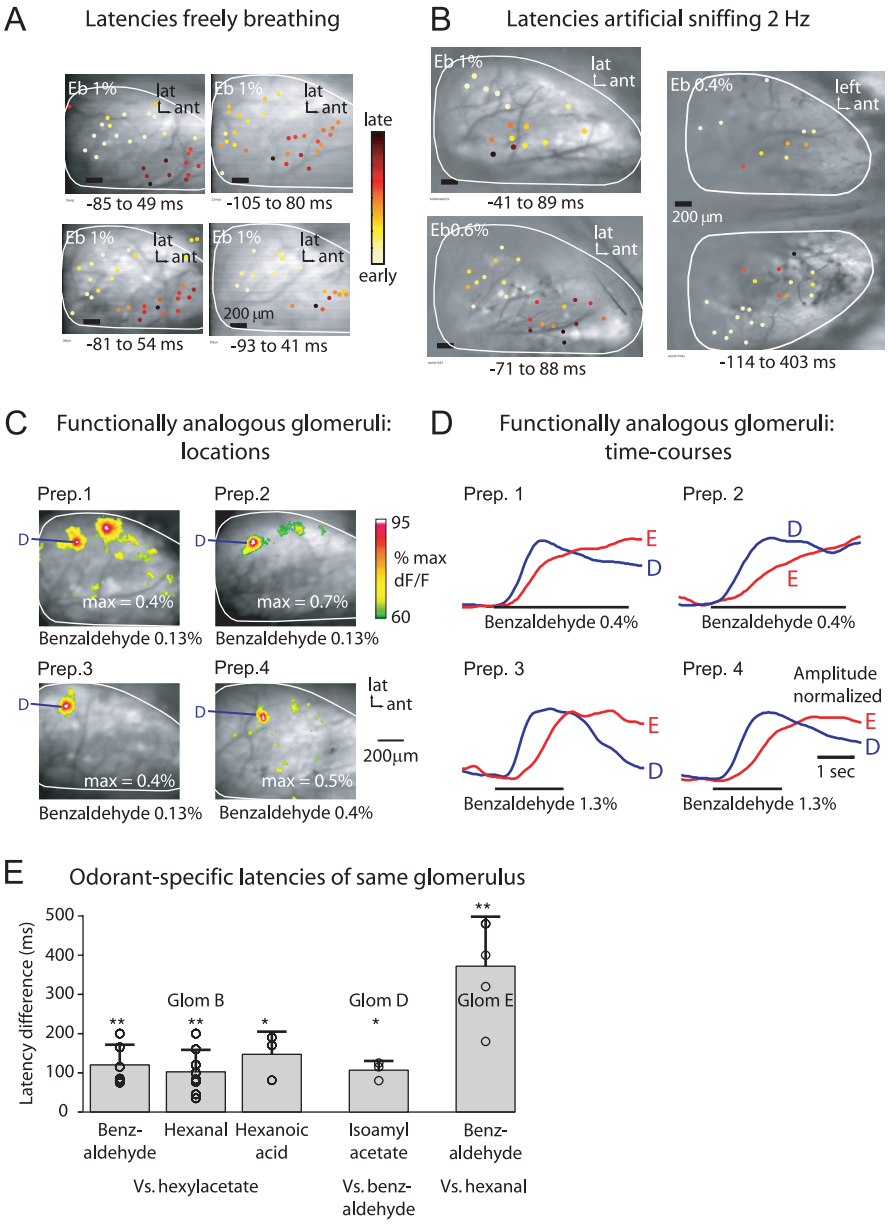

Figure 7. Consistency of spatiotemporal glomerular response properties across individuals. ***A***, Spatial distribution of relative response latencies (t_{50}) after stimulation with ethyl butyrate in four different freely breathing mice (compare Fig. 6*C*). ***B***, Spatial distribution of relative response latencies after stimulation with ethyl butyrate in three different mice under artificial sniff conditions. ***C***, Location of glomerulus D, identified by its response to a low concentration of benzaldehyde, in four different animals. ***D***, Responses of identified glomeruli D and E to benzaldehyde in four different animals. Animals were tracheotomized and odorants were delivered to the nasal epithelium by artificial sniffing (see Materials and Methods). Traces were temporally low-pass filtered (1 Hz cutoff, low-pass Gaussian filter kernel with low sharpness) to emphasize slow temporal differences and normalized to their maximum. ***E***, Response latencies of three identified glomeruli (B, D, E) in different animals, relative to the latency of response to a reference odorant for each glomerulus. The latency in response to the reference odorant was subtracted for each animal. Error bars represent SD. Significant differences between latencies in response to reference and test odorants were determined by a one-tailed Student's *t* test. Significance levels: $*p < 0.05$; $**p < 0.01$. The reference odorants are benzaldehyde for glomeruli D and E, and hexyl acetate for glomerulus B. Eb, Ethyl butyrate; Glom, glomerulus; Prep., preparation; lat, lateral; ant, anterior.

used to identify that glomerulus (benzaldehyde for glomeruli D and E; hexyl acetate for glomerulus B). Differences in response latencies of all three glomeruli to different odorants were consistent in direction in different animals, and were significantly different from zero when pooled across animals (Fig. 7*E*). Thus, as reported for spatial maps of glomerular activation, temporal properties of glomerular responses are consistent across animals.

Discussion

Maps of input to the olfactory bulb are dynamic

By selectively imaging calcium signals from ORN axon terminals, we found that odorant-evoked input to the dorsal OB is temporally complex. The most elementary observation is that odorants can evoke diverse temporal patterns of ORN input to different glomeruli. The magnitude and diversity of temporal input patterns is such that these dynamics are likely to shape postsynaptic OB activity, suggesting that the spatiotemporal patterns of OB activity noted in many previous studies are not solely a result of postsynaptic interactions in the OB network. An important result is that odorant response maps in the dorsal OB evolve over time in an odorant-specific manner. The temporal sequence of activation of different glomeruli is similar across animals and partially preserved across concentrations in subsets of glomeruli. Moreover, temporal response properties, especially response latency, were only weakly correlated with response magnitude of individual glomeruli. Hence, the dynamics of sensory input to the OB has the potential to increase the amount of information encoded by glomerular activity patterns (Gawne et al., 1996; Richmond et al., 1997).

Individual glomeruli differed mostly in the latency and rise time of their response to odorant stimulation. In general, glomeruli responding with short latencies also showed strong sniffing-related response modulation. The majority of the changes in glomerular activity maps occurred during the first 100–200 ms after response onset (i.e., during the first sniff). Awake rats and mice can perform simple odorant discrimination tasks based on sensory information obtained during this time window (Karpov, 1980; Goldberg and Moulton, 1987; Uchida and Mainen, 2003; Abraham et al., 2004). In addition, response maps can also evolve over multiple sniff cycles, as do temporal patterns of postsynaptic activity (Meredith, 1986; Wellis et al., 1989; Luo and Katz, 2001). These slower dynamics may be exploited for more difficult odor discrimination tasks, which require longer discrimination times (Slotnick and Nigrosh, 1974; Wise and Cain, 2000; Abraham et al., 2004), or for odorant discriminations at low concentrations (Youngentob et al., 1987; Wise and Cain, 2000). In addition, temporally evolving patterns of OB activity may subserve functions beyond simple discrimination, such as separating odorant components from a mixture (Jinks et al., 1998) or enhancing odorant classifications (Ambros-Ingerson et al., 1990).

Mechanisms underlying temporal patterning of glomerular inputs

It is unlikely that the observed diversity of response time courses results from differences in dye loading or calcium buffering in ORN terminals between glomeruli. Temporal response patterns of individual glomeruli were odorant specific, even for responses of similar amplitude, and responses of functionally analogous glomeruli were consistent between animals. Hence, although the calcium indicator may distort the actual dynamics of action potential firing across different populations of ORNs, our results indicate that these dynamics are ultimately determined by a combination of receptor neuron type, odorant identity, and odorant sampling behavior.

Some differences in response dynamics among ORNs may be accounted for by the relative affinity of a receptor for a particular odorant. In many systems, more effective stimuli cause both larger amplitude and shorter latency responses in sensory neurons because of stronger activation of signal transduction processes. Consistent with these effects, response latency decreased slightly with increasing concentration of the same odorant. In general, however, response amplitude and latency were only weakly correlated across different odorants and glomeruli. Moreover, we observed numerous examples in which glomeruli with a lower sensitivity to an odorant were activated more rapidly than glomeruli with higher sensitivity. The observed temporal response patterns can therefore not be explained solely by the strength of activation of signal transduction.

Receptor-specific differences in the dynamics of chemosensory transduction may also account for some of the diversity of temporal response patterns. Receptor identity determines not only odorant specificity but also temporal response features in *Drosophila* ORNs (Hallem et al., 2004). The possibility of multiple odorant-activated transduction pathways in the same ORN, as recently demonstrated in mammals, also provides a potential molecular mechanism for generating diversity in temporal responses in the periphery (Spehr et al., 2002; Lin et al., 2004).

Odorant-specific glomerular response time courses may also be generated by the sorption of vapor phase odorants onto the olfactory epithelium during inhalation and exhalation. Such chromatographic effects impose odorant-specific spatiotemporal patterns of activation onto ORNs (Kent et al., 1996) and can be pronounced in mammals with complex nasal cavities and airflow patterns. However, a detailed assessment of the influence of odorant sorption on the response dynamics of ORNs and glomeruli in mice requires additional insights into the distribution of specific ORNs and into the dynamics of nasal airflow patterns in behaving animals.

Presynaptic inhibition of calcium influx into the ORN axon terminal may also shape the dynamics of glomerular input. Presynaptic calcium influx and, consequently, transmitter release are suppressed by feedback inhibition from GABA and dopaminergic interneurons in the glomerular layer (Wachowiak and Cohen, 1999; Aroniadou-Anderjaska et al., 2000; Ennis et al., 2001; McGann et al., 2005). In slice preparations, this inhibition is maximal at 50–100 ms after olfactory nerve stimulation and decays over the next 500–1000 ms (Wachowiak et al., 2005). Glomerulus-specific temporal patterns of input could arise if the feedback presynaptic inhibition circuit showed functional variations across glomeruli.

Temporal patterning in glomerular sensory input and neurons of the OB

In OB neurons postsynaptic to glomerular afferents, temporal patterning is observed on multiple time scales. On a fast (millisecond) time scale, odorants evoke oscillatory population activity in the beta and gamma frequency ranges (Adrian, 1950; Gray, 1994; Martin et al., 2004) that is likely to be generated by neuronal circuits within the OB (Dorries and Kauer, 2000; Lagier et al., 2004) and develops over time (Adrian, 1950; Lam et al., 2000). On a slower (0.1–1 s) time scale, complex temporal patterning of odorant-evoked activity has been recorded from individual mitral cells (Macrides and Chorover, 1972; Kauer, 1974; Chaput and Holley, 1980; Pager, 1985; Meredith, 1986; Wellis et al., 1989; Buonviso et al., 1992; Chaput et al., 1992; Laurent, 2002; Leh-

mkuhle et al., 2003). Our data indicate that dynamic patterns of sensory input are one mechanism involved in the temporal patterning of postsynaptic activity in the OB. Odorant-evoked spatiotemporal activity patterns have previously been analyzed in rats by voltage-sensitive dye imaging (Spors and Grinvald, 2002). This technique predominantly detects the activity of neurons postsynaptic to glomerular inputs (Spors and Grinvald, 2002) and revealed a spatiotemporal structure of activity similar to that observed in glomerular inputs, although latency differences appeared smaller. A quantitative comparison to these data is complicated because different activity indicators, odorants, anesthetics, and species were used. However, the results are consistent with the assumption that temporal patterning of central neuronal responses is influenced by the temporal structure of sensory input. In addition, synaptic interactions in the OB are likely to contribute to the slower temporal patterning of mitral cell activity (Laurent, 2002; Urban and Sakmann, 2002).

The coupling of mitral cell activity to the respiratory rhythm has been hypothesized to play a role in information processing (Macrides and Chorover, 1972; Chaput et al., 1992; Cang and Isaacson, 2003; Margrie and Schaefer, 2003). Our results show that already at the level of primary sensory input to the olfactory bulb, the extent to which activity is coupled to respiration varies between glomeruli and regions of the bulb in a stimulus-specific manner. We also found that the extent of coupling depends on odorant sampling parameters: sequences of glomerular activation were repeated with each successive respiratory cycle at low sniff frequencies, but when sniff frequency was increased to 5 Hz, respiration modulation was substantially reduced. This finding suggests that coupling of odorant-evoked activity to respiration may be diminished or absent in some glomeruli during exploratory sniffing in awake animals. One limitation of the present study, however, is that anesthesia, temporal filtering by the calcium-sensitive dye, and limitations of airflow modulation in the artificial sniff preparation may decrease the respiration modulation observed at higher sniffing frequencies. It is therefore necessary to examine temporal patterning of activity as a function of sniffing behavior in awake animals.

Information coding by dynamic glomerular activity patterns

Patterns of relative glomerular response latencies were odorant specific, consistent across animals, and occurred mainly during the first 200 ms of an odorant response. Theoretically, such dynamic response maps could encode odorant information in different ways. For example, the brain may recognize the temporal sequence of glomerular activity patterns, as in the analysis of movies or syllables, or it may analyze instantaneous patterns within the sequence. Odorant information may also be encoded by the phase of mitral cell firing relative the respiratory cycle (Chaput et al., 1992; Hopfield, 1995; Margrie and Schaefer, 2003). Our results now demonstrate that temporal patterning exists even at the level of primary sensory input to the glomeruli. It will thus be important to incorporate the dynamics of input to the OB into models of olfactory coding and processing.

References

Abraham NM, Spors H, Carleton A, Margrie TW, Kuner T, Schaefer AT (2004) Maintaining accuracy at the expense of speed; stimulus similarity defines odor discrimination time in mice. Neuron 44:865–876.

Adrian ED (1950) The electrical activity of the mammalian olfactory bulb. Electroencephalogr Clin Neurophysiol 2:377–388.

Ambros-Ingerson J, Granger R, Lynch G (1990) Simulation of paleocortex performs hierarchical clustering. Science 247:1344–1348.

Aroniadou-Anderjaska V, Zhou FM, Priest CA, Ennis M, Shipley MT (2000) Tonic and synaptically evoked presynaptic inhibition of sensory input to the rat olfactory bulb via $GABA_B$ heteroreceptors. J Neurophysiol 84:1194–1203.

Belluscio L, Katz LC (2001) Symmetry, stereotypy, and topography of odorant representations in mouse olfactory bulbs. J Neurosci 21:2113–2122.

Bozza T, Feinstein P, Zheng C, Mombaerts P (2002) Odorant receptor expression defines functional units in the mouse olfactory system. J Neurosci 22:3033–3043.

Bozza T, McGann JP, Mombaerts P, Wachowiak M (2004) In vivo imaging of neuronal activity by targeted expression of a genetically encoded probe in the mouse. Neuron 42:9–21.

Buonviso N, Chaput MA, Berthommier F (1992) Temporal pattern analyses in pairs of neighboring mitral cells. J Neurophysiol 68:417–424.

Cang J, Isaacson JS (2003) *In vivo* whole-cell recording of odor-evoked synaptic transmission in the rat olfactory bulb. J Neurosci 23:4108–4116.

Chaput M, Holley A (1980) Single unit responses of olfactory bulb neurones to odour presentation in awake rabbits. J Physiol (Paris) 76:551–558.

Chaput MA, Buonviso N, Berthommier F (1992) Temporal patterns in spontaneous and odor-evoked mitral cell discharges recorded in anesthetized freely breathing animals. Eur J Neurosci 4:813–822.

Cinelli AR, Hamilton KA, Kauer JS (1995) Salamander olfactory-bulb neuronal-activity observed by video-rate, voltage-sensitive dye imaging. 3. Spatial and temporal properties of responses evoked by odorant stimulation. J Neurophysiol 73:2053–2071.

Digital Signal Processing Committee (1979) Algorithm 8.1. In: Programs for digital signal processing. New York: IEEE.

Dorries KM, Kauer JS (2000) Relationships between odor-elicited oscillations in the salamander olfactory epithelium and olfactory bulb. J Neurophysiol 83:754–765.

Duchamp-Viret P, Chaput MA, Duchamp A (1999) Odor response properties of rat olfactory receptor neurons. Science 284:2171–2174.

Ennis M, Zhou FM, Ciombor KJ, Aroniadou-Anderjaska V, Hayar A, Borrelli E, Zimmer LA, Margolis F, Shipley MT (2001) Dopamine D2 receptor-mediated presynaptic inhibition of olfactory nerve terminals. J Neurophysiol 86:2986–2997.

Ezeh PI, Davis LM, Scott JW (1995) Regional distribution of rat electroolfactogram. J Neurophysiol 73:2207–2220.

Firestein S, Picco C, Menini A (1993) The relation between stimulus and response in olfactory receptor-cells of the tiger salamander. J Physiol (Lond) 468:1–10.

Fried HU, Fuss SH, Korsching SI (2002) Selective imaging of presynaptic activity in the mouse olfactory bulb shows concentration and structure dependence of odor responses in identified glomeruli. Proc Natl Acad Sci USA 99:3222–3227.

Friedrich RW, Korsching SI (1997) Combinatorial and chemotopic odorant coding in the zebrafish olfactory bulb visualized by optical imaging. Neuron 18:737–752.

Friedrich RW, Laurent G (2001) Dynamic optimization of odor representations by slow temporal patterning of mitral cell activity. Science 291:889–894.

Gawne TJ, Kjaer TW, Richmond BJ (1996) Latency: another potential code for feature binding in striate cortex. J Neurophysiol 76:1356–1360.

Goldberg SJ, Moulton DG (1987) Olfactory bulb responses telemetered during an odor discrimination task in rats. Exp Neurol 96:430–442.

Gray CM (1994) Synchronous oscillations in neuronal systems: mechanisms and functions. J Comput Neurosci 1:11–38.

Guthrie KM, Anderson AJ, Leon M, Gall C (1993) Odor-induced increases in c-*fos* messenger-RNA expression reveal an anatomical unit for odor processing in olfactory-bulb. Proc Natl Acad Sci USA 90:3329–3333.

Hallem EA, Ho MG, Carlson JR (2004) The molecular basis of odor coding in the *Drosophila* antenna. Cell 117:965–979.

Hildebrand JG, Shepherd GM (1997) Mechanisms of olfactory discrimination: converging evidence for common principles across phyla. Annu Rev Neurosci 20:595–631.

Hopfield JJ (1995) Pattern-recognition computation using action-potential timing for stimulus representation. Nature 376:33–36.

Jinks A, Laing DG, Hutchinson I, Oram N (1998) Temporal processing of odor mixtures reveals that identification of components takes precedence over temporal information in olfactory memory. Ann NY Acad Sci 855:834–836.

Johnson BA, Woo CC, Leon M (1998) Spatial coding of odorant features in

the glomerular layer of the rat olfactory bulb. J Comp Neurol 393:457–471.
Johnson BN, Mainland JD, Sobel N (2003) Rapid olfactory processing implicates subcortical control of an olfactomotor system. J Neurophysiol 90:1084–1094.
Karpov AP (1980) Analysis of neuron activity in the rabbit's olfactory bulb during food-acquisition behavior. In: Neural mechanisms of goal-directed behavior (Thompson RF, Hicks LH, Shvyrkov VB, eds), pp 273–282. New York: Academic.
Kauer JS (1974) Response patterns of amphibian olfactory bulb neurones to odour stimulation. J Physiol (Lond) 243:695–715.
Kauer JS, Moulton DG (1974) Responses of olfactory bulb neurones to odour stimulation of small nasal areas in the salamander. J Physiol (Lond) 243:717–737.
Kauer JS, Senseman DM, Cohen LB (1987) Odor-elicited activity monitored simultaneously from 124 regions of the salamander olfactory bulb using a voltage-sensitive dye. Brain Res 418:255–261.
Kay LM, Laurent G (1999) Odor- and context-dependent modulation of mitral cell activity in behaving rats. Nat Neurosci 2:1003–1009.
Kent PF, Mozell MM, Murphy SJ, Hornung DE (1996) The interaction of imposed and inherent olfactory mucosal activity patterns and their composite representation in a mammalian species using voltage-sensitive dyes. J Neurosci 16:345–353.
Lagier S, Carleton A, Lledo PM (2004) Interplay between local GABAergic interneurons and relay neurons generates gamma oscillations in the rat olfactory bulb. J Neurosci 24:4382–4392.
Lam YW, Cohen LB, Wachowiak M, Zochowski MR (2000) Odors elicit three different oscillations in the turtle olfactory bulb. J Neurosci 20:749–762.
Laurent G (2002) Olfactory network dynamics and the coding of multidimensional signals. Nat Rev Neurosci 3:884–895.
Lehmkuhle MJ, Normann RA, Maynard EM (2003) High-resolution analysis of the spatio-temporal activity patterns in rat olfactory bulb evoked by enantiomer odors. Chem Senses 28:499–508.
Leveteau J, MacLeod P (1966) Olfactory discrimination in the rabbit olfactory glomerulus. Science 175:170–178.
Lin W, Arellano J, Slotnick B, Restrepo D (2004) Odors detected by mice deficient in cyclic nucleotide-gated channel subunit A2 stimulate the main olfactory system. J Neurosci 24:3703–3710.
Luo M, Katz LC (2001) Response correlation maps of neurons in the mammalian olfactory bulb. Neuron 32:1165–1179.
Macrides F, Chorover SL (1972) Olfactory bulb units: activity correlated with inhalation cycles and odor quality. Science 175:84–87.
Margrie TW, Schaefer AT (2003) Theta oscillation coupled spike latencies yield computational vigour in a mammalian sensory system. J Physiol (Lond) 546:363–374.
Martin C, Gervais R, Hugues E, Messaoudi B, Ravel N (2004) Learning modulation of odor-induced oscillatory responses in the rat olfactory bulb: a correlate of odor recognition? J Neurosci 24:389–397.
McGann JP, Pirez N, Gainey MA, Muratore C, Elias AS, Wachowiak M (2005) Odorant representation are modulated by intraglomerular but not interglomerular presynaptic inhibition of olfactory sensory neurons. Neuron 48:1039–1053.
Meister M, Bonhoeffer T (2001) Tuning and topography in an odor map on the rat olfactory bulb. J Neurosci 21:1351–1360.
Meredith M (1986) Patterned response to odor in mammalian olfactory bulb: the influence of intensity. J Neurophysiol 56:572–597.
Mombaerts P, Wang F, Dulac C, Chao SK, Nemes A, Mendelsohn M, Edmondson J, Axel R (1996) Visualizing an olfactory sensory map. Cell 87:675–686.
Optican LM, Richmond BJ (1987) Temporal encoding of two-dimensional patterns by single units in primate inferior temporal cortex. III. Information theoretic analysis. J Neurophysiol 57:162–178.
Pager J (1985) Respiration and olfactory-bulb unit-activity in the unrestrained rat—statements and reappaisals. Behav Brain Res 16:81–94.
Reisert J, Matthews HR (2001) Response properties of isolated mouse olfactory receptor cells. J Physiol (Lond) 530:113–122.
Ressler KJ, Sullivan SL, Buck LB (1994) Information coding in the olfactory system—evidence for a stereotyped and highly organized epitope map in the olfactory-bulb. Cell 79:1245–1255.
Richmond BJ, Gawne TJ, Jin GX (1997) Neuronal codes: reading them and learning how their structure influences network organization. Biosystems 40:149–157.
Rubin BD, Katz LC (1999) Optical imaging of odorant representations in the mammalian olfactory bulb. Neuron 23:499–511.
Sachse S, Galizia CG (2002) Role of inhibition for temporal and spatial odor representation in olfactory output neurons: a calcium imaging study. J Neurophysiol 87:1106–1117.
Sachse S, Rappert A, Galizia CG (1999) The spatial representation of chemical structures in the antennal lobe of honeybees: steps towards the olfactory code. Eur J Neurosci 11:3970–3982.
Slotnick BM, Nigrosh BJ (1974) Olfactory stimulus control evaluated in a small animal olfactometer. Percept Mot Skills 39:583–597.
Spehr M, Wetzel CH, Hatt H, Ache BW (2002) 3-Phosphoinositides modulate cyclic nucleotide signaling in olfactory receptor neurons. Neuron 33:731–739.
Spors H, Grinvald A (2002) Spatio-temporal dynamics of odor representations in the mammalian olfactory bulb. Neuron 34:301–315.
Stewart WB, Kauer JS, Shepherd GM (1979) Functional-organization of rat olfactory-bulb analyzed by the 2-deoxyglucose method. J Comp Neurol 185:715–734.
Strotmann J, Conzelmann S, Beck A, Feinstein P, Breer H, Mombaerts P (2000) Local permutations in the glomerular array of the mouse olfactory bulb. J Neurosci 20:6927–6938.
Uchida N, Mainen ZF (2003) Speed and accuracy of olfactory discrimination in the rat. Nat Neurosci 6:1224–1229.
Urban NN, Sakmann B (2002) Reciprocal intraglomerular excitation and intra- and interglomerular lateral inhibition between mouse olfactory bulb mitral cells. J Physiol (Lond) 542:355–367.
Vassar R, Chao S, Sitcher, Nunez JM, Vosshall LB, Axel R (1994) Topographic organization of sensory projections to the olfactory-bulb. Cell 79:981–991.
Wachowiak M, Cohen LB (1999) Presynaptic inhibition of primary olfactory afferents mediated by different mechanisms in lobster and turtle. J Neurosci 19:8808–8817.
Wachowiak M, Cohen LB (2001) Representation of odorants by receptor neuron input to the mouse olfactory bulb. Neuron 32:723–735.
Wachowiak M, Cohen LB (2003) Correspondence between odorant-evoked patterns of receptor neuron input and intrinsic optical signals in the mouse olfactory bulb. J Neurophysiol 89:1623–1639.
Wachowiak M, Denk W, Friedrich RW (2004) Functional organization of sensory input to the olfactory bulb glomerulus analyzed by two-photon calcium imaging. Proc Natl Acad Sci USA 101:9097–9102.
Wachowiak M, McGann JP, Heyward PM, Shao Z, Puche AC, Shipley MT (2005) Inhibition of olfactory receptor neuron input to olfactory bulb glomeruli mediated by suppression of presynaptic calcium influx. J Neurophysiol 94:2700–2712.
Wellis DP, Scott JW, Harrison TA (1989) Discrimination among odorants by single neurons of the rat olfactory-bulb. J Neurophysiol 61:1161–1177.
Wise PM, Cain WS (2000) Latency and accuracy of discriminations of odor quality between binary mixtures and their components. Chem Senses 25:247–265.
Xu F, Kida I, Hyder F, Shulman RG (2000) Assessment and discrimination of odor stimuli in rat olfactory bulb by dynamic functional MRI. Proc Natl Acad Sci USA 97:10601–10606.
Xu F, Liu N, Kida I, Rothman DL, Hyder F, Shepherd GM (2003) Odor maps of aldehydes and esters revealed by functional MRI in the glomerular layer of the mouse olfactory bulb. Proc Natl Acad Sci USA 100:11029–11034.
Youngentob SL, Mozell MM, Sheehe PR, Hornung DE (1987) A quantitative analysis of sniffing strategies in rats performing odor detection tasks. Physiol Behav 41:59–69.